Osteoarthritis and Cartilage 30 (2022) 1593–1605

Osteoarthritis and Cartilage

Subchondral bone structure and synovial fluid metabolism are altered in injured and contralateral limbs 7 days after non-invasive joint injury in skeletally-mature C57BL/6 mice

B.D. Hislop [†], C. Devine [‡], R.K. June [† §], C.M. Heveran [† *]

† *Department of Mechanical & Industrial Engineering, Montana State University, USA*
‡ *Department of Chemical & Biological Engineering, Montana State University, USA*
§ *Department of Microbiology & Cell Biology, Montana State University, USA*

ARTICLE INFO

Article history:
Received 19 April 2022
Accepted 4 September 2022

Keywords:
Subchondral bone
Synovial fluid
Post-traumatic osteoarthritis
Metabolomics
Nanoindentation

SUMMARY

Objective: Post-traumatic osteoarthritis (PTOA) commonly develops after ACL injury, but early changes to the joint soon after injury are insufficiently understood. The objectives of this study were (1) evaluate the response of subchondral bone tissue modulus to joint injury and (2) identify which bone structural, material, and metabolic outcomes are local (i.e., injured joint only) or systemic (i.e., injured and contralateral-to-injured).

Design: Female C57Bl\6N mice (19 weeks at injury) underwent tibial compression overload to simulate ACL injury ($n = 8$) or a small pre-load ($n = 8$). Synovial fluid was harvested at euthanasia 7 days later for metabolomic profiling. Bone outcomes included epiphyseal and SCB microarchitecture, SCB nanoindentation modulus, SCB formation rate, and osteoclast number density.

Results: Injury decreased epiphyseal bone volume fraction ([-5.29, −1.38%], $P = 0.0016$) and decreased SCB thickness for injured vs sham-injured limbs ([2.2, 31.4 μm], $P = 0.017$)). Epiphyseal bone loss commonly occurred for contralateral-to-injured limbs. There was not sufficient evidence to conclude that SCB modulus changes with injury. Metabolomic analyses revealed dysregulated synovial fluid metabolism with joint injury but that many metabolic pathways are shared between injured and contralateral-to-injured limbs.

Conclusion: This study demonstrates rapid changes to bone structure and synovial fluid metabolism after injury with the potential for influencing the progression to PTOA. These changes are often evidenced in the contralateral-to-injured limb, indicating that systemic musculoskeletal responses to joint injury should not be overlooked.

© 2022 Osteoarthritis Research Society International. Published by Elsevier Ltd. All rights reserved.

Introduction

Post-traumatic osteoarthritis (PTOA) affects 5.6 million people in the US each year[1]. Patients who suffer ACL tears develop PTOA at an alarming rate. Regardless of ACL reconstruction status, 50% of patients will develop PTOA within 20 years of joint injury[2]. Early interventions that mitigate the first deleterious changes to joint tissues may relieve some of the immense physical and financial burdens of PTOA[3–5]. However, to design and implement early interventions, additional data are needed to improve the understanding of how the loading and biological environments of the injured knee change early after joint injury.

It is well-established that subchondral and epiphyseal bone undergo transient thinning after joint injury that later reverses and progresses towards sclerosis[6–10] (Table I). The rapid decline of subchondral bone and epiphyseal microarchitecture may directly impact the bone mechanical environment. If subchondral and epiphyseal bone microarchitecture decreases, μstrain will increase in subchondral bone with potential impacts to bone mechanotransduction[11,12]. The changes would be expected to be further exacerbated by changes to tissue-scale subchondral bone modulus, since the stiffness of bone tissue influences the strain experienced by osteocytes, a bone cell type recently implicated in the

* Address correspondence and reprint requests to: C.M. Heveran, Department of Mechanical & Industrial Engineering, Montana State University, USA. Tel: 1 406-994-2010.
E-mail address: chelsea.heveran@montana.edu (C.M. Heveran).

https://doi.org/10.1016/j.joca.2022.09.002
1063-4584/© 2022 Osteoarthritis Research Society International. Published by Elsevier Ltd. All rights reserved.

Study	Animal sex, strain, and species	Animal age (weeks)	Injury model	Evaluation timepoints (days after injury)	Regions of interest	Early acute epiphysial bone response to injury (7-10d)
Christiansen *et al.*, Osteoarthritis and Cartilage, (2012), 773–782, 20 (7)[8]	Male C57BL/6N mice	10	Non-invasive ACL rupture via tibial compression overload	1, 3, 7, 14, 28, 56	Distal femoral epiphysis, proximal tibial epiphysis	*Distal femoral epiphysis* 7d (injured vs contralateral limb): • 44% ↓BV/TV • 25% ↓Apparent BMD • 24% ↓ Tb.Th *Proximal tibial epiphysis* 7d (injured vs contralateral limb): • 40% ↓ BV/TV • 20% ↓ Apparent BMD • 15% ↓ Tb.Th *Subchondral bone plate* • 7%↓ Scb.Th
Anderson *et al.*, Journal of Orthopaedic Research, (2016)[6]	Female C57BL/6N mice	10	Non-invasive ACL rupture via tibial compression overload	7, 14	Distal femoral epiphysis	7d (injured vs sham-injured limb): • 25% ↓BV/TV • 20% ↓ Tb.Th
Khorasani *et al.*, Arthritis Research and Therapy, (2015), 17 (1)[9]	Female C57BL/6N mice	10	Non-invasive ACL rupture via tibial compression overload	7, 14, 56	Distal femoral epiphysis	7d (injured vs sham-injured limb): •27% ↓ BV/TV •18% ↓Tb.Th
Lockwood *et al.*, Journal of Orthopaedic Research, (2014), 79–88, 32 (1)[7]	Male C57BL/6N mice	11	Non-invasive ACL rupture via tibial compression overload	10, 84, 112	Distal femoral epiphysis	*High strain rate (*500 mm/s*)* 10d (injured vs sham-injured limb): •20% ↓ BV/TV *Low strain rate (*1 mm/s*)* 10d (injured vs sham-injured limb): • 31% ↓ BV/TV
Wegner *et al., Journal of Orthopaedic Research, (2019), 2,429–2,436, 37(11)*[10]	Female C57BL/6N mice	10	Non-invasive ACL rupture via tibial compression overload	7	Distal femoral epiphysis	7d (injured vs contralateral limb): • ~18% ↓ BV/TV
Hahn *et al.*, Osteoarthritis and Cartilage, (2021), 882–893, 29 (6)[25]	Male, Female C57BL/6 mice	20	Non-invasive ACL rupture via tibial compression overload	7	Distal femoral epiphysis	7d (injured vs contralateral limb): • 5.9 % ↓ Tb.Th • 7% ↑ BS/BV
Maerz *et al., Journal of Orthopaedic Research, (2021), 1965–1976, 39(9)*[27]	Female Lewis rat	14	Non-invasive ACL rupture via tibial compression overload	3, 7, 10, 14	Distal femoral epiphysis	*Medial condyle* 7d (injured vs ipsilateral sham-injured limb) •~3% ↓ BV/TV 7d (injured vs contralateral limb) •~3% ↓ Scb.Th *Lateral condyle* 3d (injured vs contralateral limb) •~2% ↑ BV/TV •~2% ↑ Scb TMD 7d (injured vs contralateral limb) •~2% ↑ BV/TV
McCulloch *et al.*, Osteoarthritis and Cartilage, (2019), 1800–1810, 27 (12)[23]	Male C57BL/6 mice	10	Destabilized medial meniscectomy	7, 14, 28	Proximal tibial epiphysis	7d (injured vs contralateral limb): •~48% ↑ BV/TV
Das Neves Borges, Vincent, and Marenzana, PLoS ONE, (2017), 12 (3)[22]	Male C57BL/6 mice	10	Destabilized medial meniscectomy	7, 14, 28, 56, 84, 140	Proximal tibial epiphysis	*Medial condyle* 7d (injured vs contralateral limb): •~3% ↑ BV/TV
White, Brancati, and Lepley, Journal of Orthopaedic Research, (2022), 74–86, 40 (1)[17]	Male, Female Long-Evans Rat	16	Destabilized medial meniscectomy	7, 14, 28, 56	Distal femoral epiphysis	*Medial condyle* 7d (injured vs uninjured control rats): •*Male*: ~167% ↑ Scb.Pl.Po •Female: ~90% ↑ Scb.Pl.Po *Lateral condyle* 7d (injured vs uninjured control rats): •*Male*: ~263% ↑ Scb.Pl.Po

Table 1 (*continued*)

Study	Animal sex, strain, and species	Animal age (weeks)	Injury model	Evaluation timepoints (days after injury)	Regions of interest	Early acute epiphysial bone response to injury (7-10d)
						•*Female*: ~154% ↑ Scb.Pl.Po

BV/TV, Trabecular bone volume per tissue volume; BMD, Bone mineral density; BA, Bone area; Tb.Th, Trabecular thickness; BS/BV, Bone surface per bone volume; TMD, Tissue mineral density; Scb.Th, Subchondral bone plate thickness; Scb.Pl.Po, Subchondral bone plate porosity.

Table 1

Literature review of early bone response to ACL injury in rodent models

Osteoarthritis and Cartilage

development of PTOA[13,14]. Subchondral bone modulus decreases for rodents when osteoarthritis is established and the subchondral bone plate is sclerotic[15,16]. However, it is unknown whether subchondral bone modulus changes coincide with subchondral bone plate thinning. Thus, it is critical to quantify subchondral bone modulus changes after joint injury to better understand the effects of early bone changes on the bone tissue mechanics and mechanotransduction.

The impacts of joint injury may extend to the contralateral-to-injured limb. Patients who undergo an initial knee replacement have a 37.2% chance of needing a contralateral limb replacement within 10 years[15]. Christiansen and coauthors found decreased trabecular bone volume fraction in the contralateral epiphysis 7d after non-invasive joint injury in mice[8]. In another study, the same authors found decreased trabecular microarchitecture in the L5 vertebra 10 days after joint injury[16]. Contralateral bone loss may be the consequence of altered loading[17], a systemic inflammatory response[18,19], or altered remodeling bone cell populations[13,20,21]. However, rodent models of PTOA commonly only compare early outcomes after joint injury between injured and contralateral-to-injured limbs and not to a sham-injured control[8,10,22,23]. Comparisons between injured and sham-injured limbs are usually limited to later time points when bone is sclerotic and PTOA is established[8,22,23]. Important gaps remain in our understanding of early bone changes in the injured and contralateral-to-injured limbs.

Synovial fluid interacts with multiple joint tissues including bone and cartilage. Therefore, shifts in synovial fluid metabolism marked by changes in metabolites (i.e., small molecules chemically changed in metabolism) could point to specific biological changes that rapidly occur after ACL injury. These potential biomarkers would likely be useful for designing early interventions to mitigate the progression to PTOA. Furthermore, synovial fluid, unlike other joint tissues, can potentially be assessed through needle biopsy in a clinical setting[24]. Recent studies find distinct metabolic profiles between injured and sham-injured synovial fluid 7d after joint injury in mouse models[25,26]. However, what shifts in synovial fluid metabolism occur locally (i.e., injured joint) or also systemically (i.e., also present in contralateral joint) soon after injury remain unknown. Furthermore, since synovial fluid interfaces with bone, which is much more metabolically active than cartilage[27], it is of key interest to understand whether shifts in synovial fluid metabolism occur at the same time as early changes to bone structure and material properties.

In this study, we fill several significant critical gaps about the early biological and structural response of the joint 7 days after ACL injury. First, we test whether subchondral bone tissue material properties change in the same time frame as bone thinning. Next, we evaluate shifts in synovial fluid metabolism as an indication of changes to cellular bioenergetics of the joint. All structural, material, and biological outcomes are compared between injured, contralateral-to-injured, and sham-injured joints, allowing estimation of local (i.e., injured joint only) and systemic (i.e., injured and contralateral-to-injured) effects.

Materials and methods

Mouse model of joint injury

All animal procedures were approved by the Montana State University Institutional Animal Care and Use Committee. C57Bl\6N mice were acquired from Charles River laboratories. Mice were allowed to acclimate for 2 weeks prior to injury (19-weeks old at injury). Each mouse was assigned to either the injury (overload-induced ACL tear) or control (sham-injury) groups. The injured or sham-injured joint was randomly assigned to a side using the sample function in R.

On the day of injury, mice were anesthetized in an inhalation chamber (2–4% isoflurane, ~30 s) and then nose cone (2% isoflurane) while one limb was loaded into a custom-built loading machine [Fig. 1(A)–(B)]. Sham-injured and injured limbs were subjected to a pre-load (1–2N, 0.5 mm/s). Injured limbs were loaded to 12–15N at 130 mm/s, consistent with prior studies [Fig. 1(C)] [7,8,28].

ACL tears were confirmed *in vivo* by a characteristic release in compressive load and by performing pre- and post-injury joint laxity tests of anterior stability[7,8,28]. Five mice were excluded for failed ACL tears and two for tibial fractures. After exclusion of these 7 mice, 8 mice were studied per treatment group (injured, sham-injured). Sixteen mice ($n = 8$ injured, $n = 8$ sham-injured) were studied for subchondral bone response and synovial fluid responses to joint injury.

Mice were group housed (≤5 mice per cage) and provided rodent diet (Purina LabDiet 5,053) and water *ad libitum*. Calcein (20 mg/kg) and alizarin (30 mg/kg) fluorochrome labels were administered intraperitoneally 2–3 days before injury and 6 days post-injury, respectively. Mice were euthanized 7 days post-injury *via* cervical dislocation.

Microarchitecture of the proximal tibia epiphysis and subchondral bone

Tibiae were cleaned of non-osseous tissue, submerged in 70% ethanol, and refrigerated (4°C). Proximal tibiae were evaluated for microarchitecture of the epiphysis and subchondral bone thickness and tissue mineral density in the medial and lateral compartments (μCT40, Scanco Medical AG, 10 μm isotropic voxel size, 70 kVP, 114 μA, 200 ms integration time). The scanned volume was a 1 mm (100 coronal slices) thick region at the center of the proximal tibial epiphysis. The first region of interest included the epiphysis [Fig. 2(C)]. Analyses included bone volume (BV, mm^3), total volume

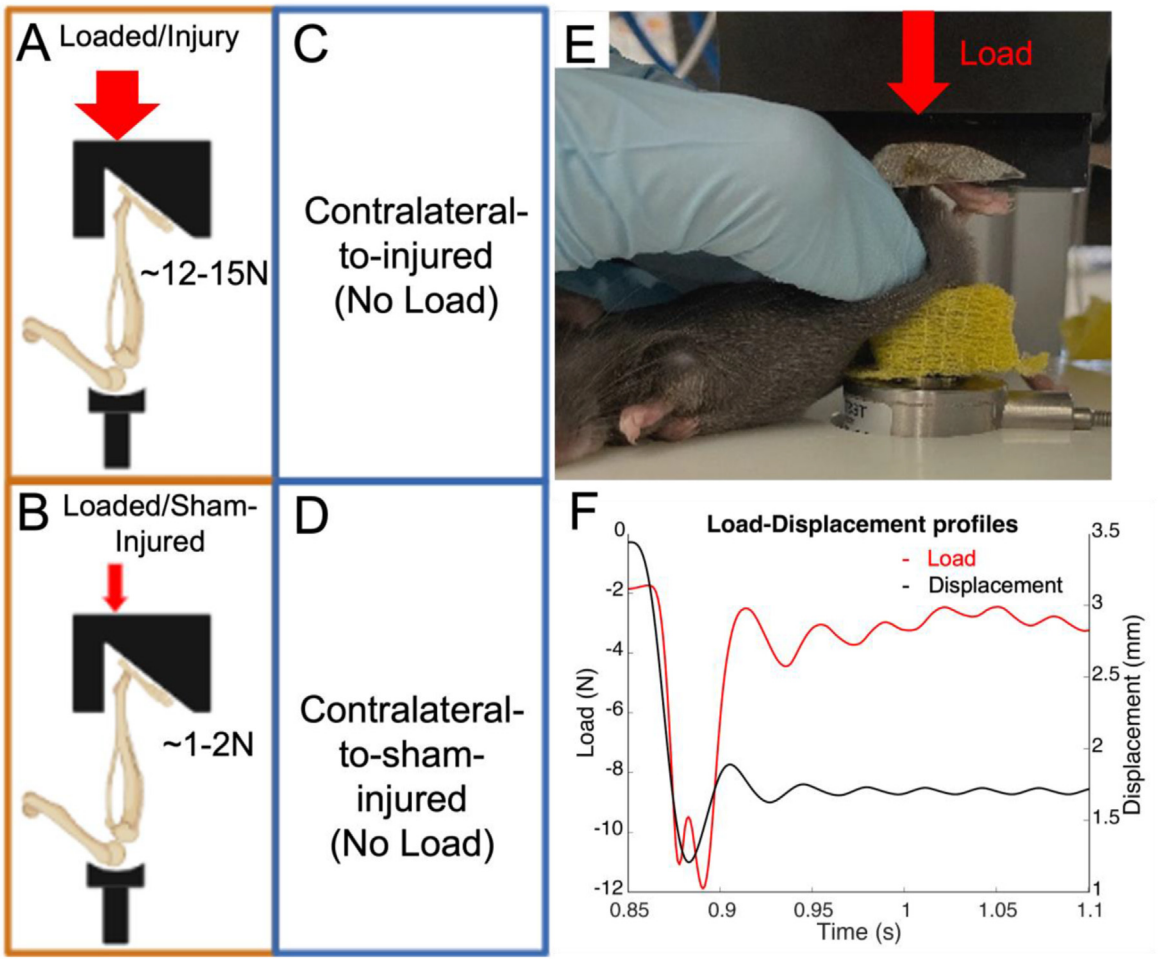


Fig. 1

Osteoarthritis and Cartilage

Mouse PTOA model. A, B) Schematic of mouse hind limb in loading machine with load applied parallel to tibia. C,D) The contralateral limbs of both injured and control mice were not loaded. E) Mouse loaded into loading machine during study. F) Load-displacement curves showing a change in displacement coinciding with a sinusoidal load response between 0.875- and 0.9-s characteristic of an anterior translation of the tibia leading to ACL rupture[8,27]. Fig. 1(A) and (B) created with Biorender.com.

(TV, mm^3), bone volume fraction (BV/TV, %), bone mineral density (BMD, $mgHA/cm^3$), trabecular number (Tb.N, 1/mm), trabecular spacing (Tb.Sp, mm), and trabecular thickness (Tb.Th, mm)[29]. Subchondral bone plate thickness and TMD were analyzed for consistent locations in the medial and lateral compartments (Scb.Th, mm; Scb.TMD, $mgHA/cm^3$) [Fig. 2(C)].

Osteoclastic bone resorption at the femoral epiphysis

Femurs were placed in 10% neutral buffered formalin for 18 h, decalcified in Ethylene Diamine Tetraacetic Acid (EDTA), dehydrated in a graded series of ethanol concentrations (70–100%), embedded in paraffin, and microtomed to 6 μm-thick sagittal sections. Sections were stained via standard protocols for tartrate resistant acid phosphatase (TRAP) and imaged using a brightfield microscope (Nikon, Eclipse E-800) [Fig. 2(B)]. Using ImageJ [30], an evaluator blinded to joint injury status traced the epiphysial trabecular bone surfaces enclosing the marrow cavities (4X images) and counted the multinucleated, TRAP-positive cells (i.e., dark pink) (10X images). We report the osteoclast number density normalized per marrow area and bone surface.

Dynamic bone remodeling of the proximal tibia epiphysis

Following microCT, tibiae were embedded in poly (methyl) methacrylate, sectioned along the coronal plane of the tibial plateau, and polished to a mirror finish as previously described (Fig. 2)[31]. Calcein and alizarin labels were imaged at the proximal tibia using confocal laser scanning microscopy (CLSM, inverted Leica SP5). Samples were excited at 488 nm and 561 nm. Emission windows were 500 nm–550 nm (calcein) and 650 nm–750 nm (alizarin). The voxel size was 1.52 μm × 1.52 μm × 4.74 μm. Z-stacks were collected for each sample in medial and lateral regions and one in-focus slice from each image stack was analyzed (Imaris 9.3.0, Bitplane).

Bone perimeter and calcein and alizarin labels were traced on iPads by two independent evaluators blinded to injury status. If inter-evaluator agreement was less than 95%, sections were re-analyzed by both evaluators. Bone perimeter and labels were

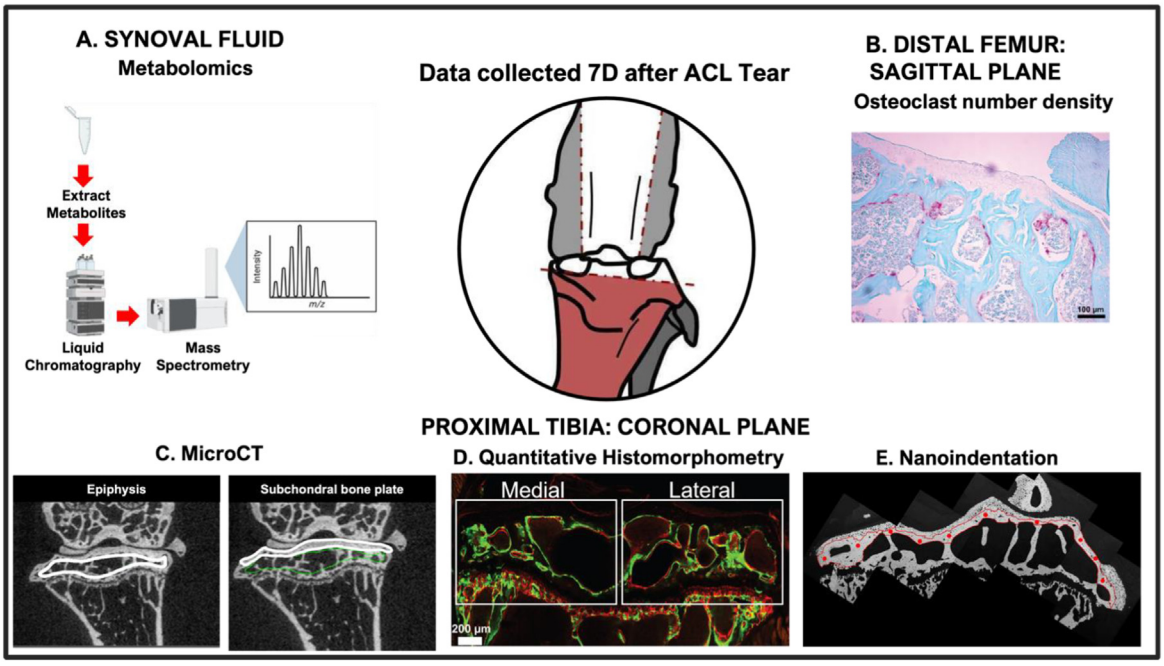


Fig. 2

Osteoarthritis and Cartilage

Schematic of experimental methods to characterize bone and synovial fluid responses to joint injury. A) Schematic of synovial fluid metabolomic extraction and analysis procedure from extraction to mass spectra. B) Osteoclast activity at the distal femur was evaluated from TRAP-stained sections. C) Microarchitecture of the epiphysis and subchondral bone were evaluated using microCT. D) Dynamic bone remodeling for the epiphysis was measured from confocal laser scanning microscopy images from polished coronal sections. Medial and lateral regions of interest are delineated by the white boxes. E) Subchondral bone modulus was measured using nanoindentation on polished coronal sections. Indents were placed within the outlined region spanning the medial to lateral aspects of the subchondral bone plate. Fig. 2(A) Created with Biorender.com.

measured in epiphyseal regions of interest [Fig. 2(D)]. For each region of interest, bone surface, alizarin surface/bone surface, and calcein surface/bone surface were calculated. These measures were calculated using a custom written MATLAB script (available at: https://github.com/hisl6802/Quantitative-Histomorphometry-Automated-Tracing-).

Tissue-scale subchondral bone plate modulus of the proximal tibia

Nanoindentation was performed on subchondral bone from polished proximal tibia sections using a KLA Tencor iMicro (5 mN max load, 30s load and unload, 60s hold) and diamond Berkovich tip (ν_t = 0.07, E_t = 1,140 GPa). Indents were placed between the tidemark and the epiphysis spanning the medial to lateral subchondral bone plate (n = 8 per sample) [Fig. 2(E)]. Indentation curves were analyzed for reduced modulus (E_r) consistent with description by Vahidi *et al.*[31] (Supplementary Data Figure S1). We report the indentation modulus E_i, which is corrected for the diamond tip properties, but avoids assuming a Poisson's ratio for the tissue sample (ν_s) [Equations (1) and (2)][32].

$$\frac{(1-\nu_s^2)}{E_s} = \left(\frac{1}{E_r} - \frac{(1-\nu_t^2)}{E_t}\right) \quad (1)$$

$$E_i = \frac{E_s}{(1-\nu_s^2)} \quad (2)$$

Indents were excluded for poor surface contact, a non-smooth loading or unloading curve, or moduli indistinguishable from PMMA ($\leq$5 GPa).

Profiling the metabolic response of joints to traumatic injury

Synovial fluid was extracted from the stifle joint immediately following euthanization consistent with our previous publication[26]. Briefly, an incision was made anteriorly into the synovium and synovial fluid was collected by adsorption using Melgisorb alginate dressing (Tendra). Metabolites were extracted as previously described[33,34] and analyzed using Liquid Chromatography-Mass Spectrometry (LC-MS, Agilent 1290 UPLC, Agilent 6538 Q-TOF mass spectrometer) [Fig. 2(A)]. Spectra were submitted to XCMS[35] for peak identification.

Data analysis

Bone outcomes

Bone measures were analyzed using mixed model analysis of variance (ANOVA). Fixed effects included injury (injury vs sham-injury) and load side (loaded and sham-loaded vs contralateral). The individual mouse was a random effect. Each model included an interaction term between load side and injury. For nanoindentation modulus, which included multiple indents per sample, the relative distance from the medial edge was included as a covariate. For fluorochrome labels and subchondral bone, location (i.e., medial or

lateral) was a fixed effect and limb was a random effect nested within the individual mouse.

Dependent variable transformations were performed, if necessary, to satisfy ANOVA assumptions of residual normality and homoscedasticity. Critical alpha was set *a priori* at 0.05. Significant interactions were followed by post-hoc tests for simple effects while maintaining family-wise error at 0.05 using a Bonferroni correction. Spearman rank correlation analysis was performed to evaluate relationships between bone outcomes and peak load.

Metabolomic analysis

ANOVA, *t*-tests, principal component analysis (PCA), partial least squares-discriminant analysis (PLS-DA), and hierarchical clustering were used to compare metabolic profiles for synovial fluid from the injured, sham-injured, and contralateral-to-injured limbs. The metabolic data were then subjected to cluster validation and ensemble clustering to determine the metabolites which consistently clustered together (Supplementary Data) (Fig. 3). The 10 largest clusters identified through ensemble clustering were submitted to mummichog to identify the associated metabolic pathways[36].

Results

Epiphyseal and subchondral bone plate microarchitecture of the proximal tibia declines

MicroCT of the tibial epiphysis revealed significant effects of injury (i.e., injury vs sham-injury) and loaded side (i.e., the injured and sham-injured limb vs the contralateral limbs) on several measures of bone microarchitecture. Epiphyseal BV/TV decreased with injury (relative change −10.8%, $P = 0.002$, 95% CI [−4.66, −1.21%]). BV/TV was also lower for loaded vs unloaded sides (−7.5%, $P = 0.023$ [−3.74, −0.29%]) [Fig. 4(A)]. Epiphyseal BMD also decreased with injury (−7.1%, $P = 0.012$ [−42.83, −5.67 mgHA/cm^3]) and for loaded sides (−5.8%, $P = 0.040$ [−38.08, −0.92 mgHA/cm^3]). Similarly, epiphyseal Tb.Th decreased with injury (−5.5%, $P = 0.028$ [−7.4e-3, −4.5e-4 mm]) and for loaded sides (−6.0%, $P = 0.017$ [−7.8e-3, -8.3e-4 mm]). For each of these measures, there were no significant interactions between injury and loaded side. Tb.N and Tb.Sp were not affected by injury, loaded side, or their interaction. Because the peak load to cause the joint injury varied between mice, we tested whether peak load influenced measures of bone microarchitecture. Spearman's rank correlation analysis of peak load vs BV/TV, BMD or Tb.Th found no significant relationships ($P > 0.05$ for all) (95% CI for ρ [−0.83, 0.537], [−0.894, 0.386], [−0.84, 0.519], respectively).

Subchondral bone plate thickness (Scb.Th) showed an interactive effect of injury and loaded side ($P = 0.039$) [Fig. 4(B)]. Post-hoc testing revealed significantly decreased Scb.Th for injured compared with sham-injured limbs (−12.3%, $P = 0.017$ [−31.4, −2.2 μm]). There may be a reduction in Scb.Th for injured compared with contralateral-to-injured limbs, but we were underpowered to detect this difference ($P = 0.054$). The Scb.Th was not different for sham-injured and contralateral-to-sham injured limbs. The subchondral bone plate thickness was on average 18 μm thicker for the medial compartment (14.5%, $P < 0.01$ [11.9,

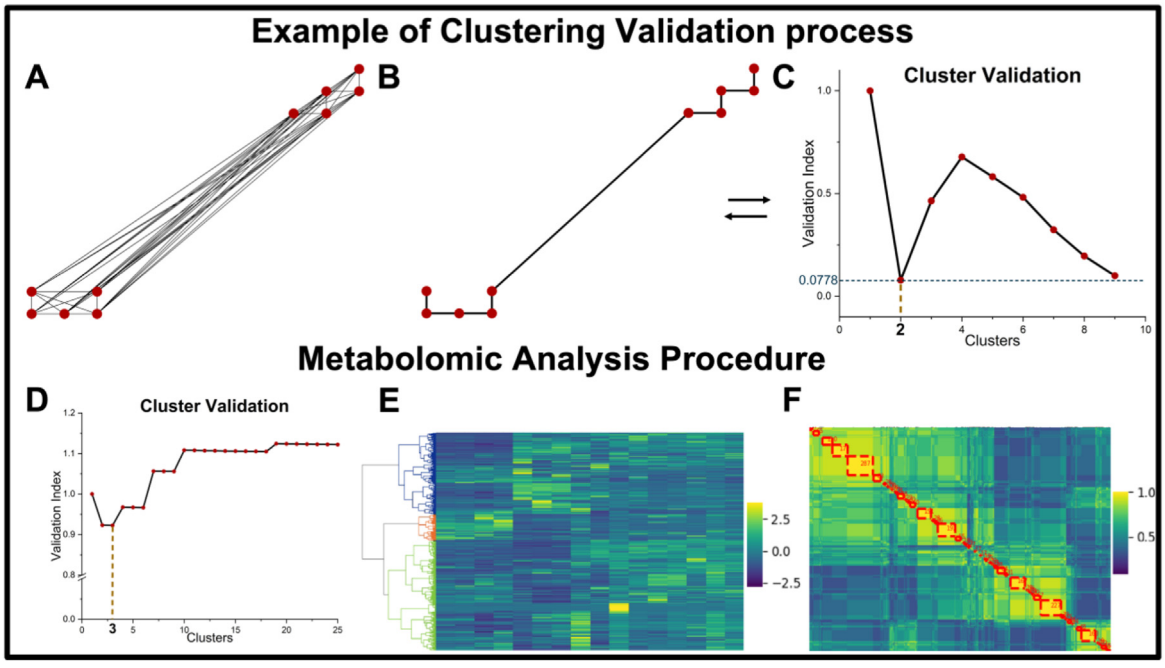


Fig. 3

Osteoarthritis and Cartilage

Example of minimum spanning tree (MST) based cluster validation. Metabolomic clustering analysis procedure. A) Ten 2D points (randomly generated using MATLAB) connected in a full dissimilarity tree. B) MST for these ten points. C) Cluster validation for B showing that 2 clusters (0.0778 validation index) is the optimum choice. D) Cluster validation output for analysis of sham-injured & injured limb metabolic profiles showing a local minimum at 3 clusters. E) Graphical representation of one of thirteen hierarchical clustering outputs of the sham-injured & injured metabolomic data, with the three clusters of interest colored (blue, orange, and green). F) Ensemble clustering output showing the clusters with greater than 40 metabolites in red dashed squares (yellow represents metabolites which clustered together in each of the thirteen clusterings).

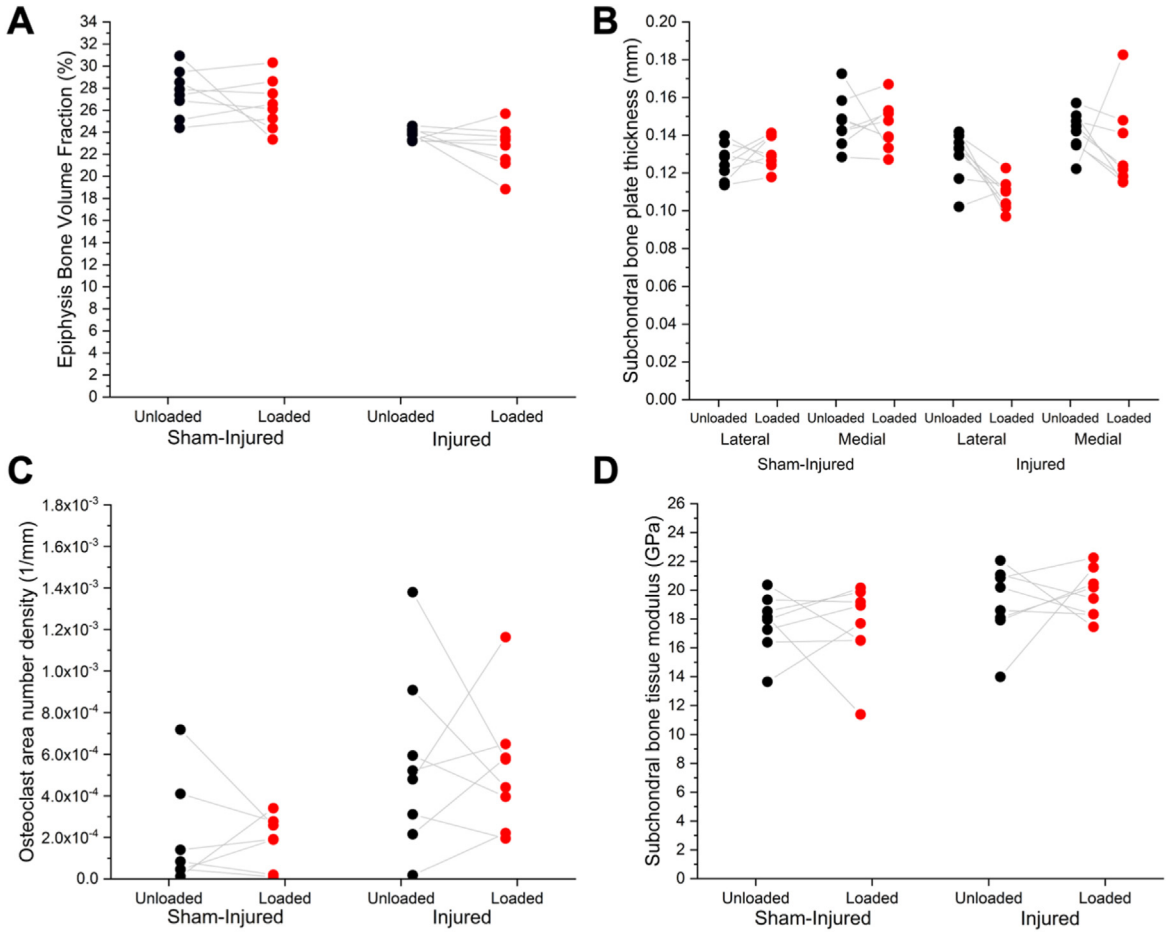


Fig. 4

Osteoarthritis and Cartilage

Key subchondral bone outcomes for loaded vs contralateral limbs for injured and sham-injured mice, including A) epiphyseal bone volume fraction, B) mean subchondral bone thickness, C) osteoclast number density per area, and D) subchondral bone tissue modulus.

24.2 μm]). Subchondral bone tissue mineral density (SCB.TMD) also showed an interactive effect of injury and loaded side ($P < 0.01$). From post-hoc tests, injured limbs had lower SCB.TMD than sham-injured (−2.3%, $P = 0.021$ [−66.8, −3.90 mgHA/cm^3]) and contralateral-to-injured limbs (−4.1%, $P = 0.015$ [−74.7, −6.68 mgHA/cm^3]). The SCB.TMD was not different for sham-injured and contralateral-to-sham injured limbs or between medial and lateral compartments. SCB.Th and SCB.TMD were not related to peak load ($P > 0.05$, ρ [−0.91, 0.22]; $P > 0.05$, ρ: [−0.88, 0.34]; respectively) (see Table II).

Osteoclastic resorption at the distal femoral epiphysis increases but proximal epiphysis bone formation is unchanged

Injury increased osteoclast area number density on average by 3.87 times, and osteoclast number per bone surface at the distal femur epiphysis on average by 3.68 times (+287.2%, $P = 0.017$ [2.7e-4, 2.33e-3 1/mm^2]; +267.4%, $P = 0.016$, [7.6e-3, 5.8e-2 1/mm], respectively) (Fig. 4(C), Table III). These measures were not impacted by loaded side nor the interaction between loaded side and injury. Thus, there was a similar increase in osteoclast abundance for both injured and contralateral-to-injured limbs. TRAP data were natural-log transformed for ANOVA analyses and back transformed for interpretation.

Loaded side affected the proximal tibia epiphysis calcein-to-bone-surface (−18.3%, $P = 0.005$ [−13.07, −2.84%]). Since calcein was administered 2–3 before injury, results indicate that bone resorption was increased for loaded (injured and sham-injured) limbs. Calcein labeling was not affected by injury, location (medial vs lateral), or the interaction of these factors. Alizarin-to-bone-surface was not affected by injury, loaded side, region of interest, or the interaction of these factors. Bone formation surface was not impacted by the joint injury, since alizarin was administered 6 days after the joint injury and 1 day before euthanasia.

Tissue-scale subchondral bone plate modulus is not changed

Nanoindentation tested whether subchondral bone plate modulus changes soon after joint injury. We first evaluated whether indent position (i.e., relative distance from the medial

Measure	**Control**		**Injured**	
	Contralateral-to-sham $n = 8$	**Sham-Loaded** $n = 8$	**Contralateral-to-injured** $n = 8$	**Loaded to injury** $n = 8$
Proximal tibia epiphysis				
Bone Volume Fraction (%) ***Injury***: $P = 0.002$ 95%CI: (−4.66, −1.21) ***Loaded side***: $P = 0.023$ 95%CI: (−3.74, −0.29) Injury x loaded side: NS	27.57 ± 2.16	26.51 ± 2.28	25.60 ± 2.91	22.63 ± 2.09
Bone Mineral Density (mgHA/cm^3) ***Injury***: $P = 0.012$ 95%CI: (−42.83, −5.67) ***Loaded side***: $P = 0.040$ 95%CI: (−38.08, −0.92) Injury x loaded side: NS	345.50 ± 21.26	337.25 ± 24.76	332.50 ± 29.57	301.75 ± 26.31
Trabecular Number (1/mm) Injury: NS 95%CI: (−0.221, 0.158) Loaded side: NS 95%CI: (−0.243, 0.136) Injury x loaded side: NS	4.05 ± 0.28	3.97 ± 0.33	3.99 ± 0.26	3.97 ± 0.13
Trabecular Thickness (mm) ***Injury***: $P = 0.028$ 95%CI: (−7.4e-3, -4.5e-4) ***Loaded side***: $P = 0.017$ 95%CI: (−7.8e-3, -8.3e-4) Injury x loaded side: NS	0.073 ± 3.9e-3	0.071 ± 5.1e-3	0.071 ± 4.6e-3	0.065 ± 5.5e-3
Trabecular Spacing (mm) Injury: NS 95%CI: (−1.5e-2, 1.6e-2) Loaded side: NS 95%CI: (−1.6e-2, 1.5e-2) Injury x loaded side: NS	0.261 ± 0.016	0.263 ± 0.032	0.264 ± 0.023	0.261 ± 0.01
Tibia subchondral bone plate				
Subchondral bone plate thickness (mm) **Injury**: $P = 0.019$ 95%CI: (−16.8, −1.21) Loaded side: NS 95%CI: (−14.3, 1.3) **Location**: $P < 0.01$ 95%CI: (11.9, 24.2) **Injury x loaded side**: $P = 0.039$ Injury x location: NS Location x loaded side: NS	0.137 ± 0.016	0.138 ± 0.012	0.135 ± 0.013	0.121 ± 0.01
Subchondral bone plate tissue mineral density (mgHA/cm^3) Injury: NS 95%CI: (−25.70, 7.89) Loaded side: NS 95%CI: (−31.10, −2.57) Location: NS 95%CI: (−3.45, 16.20) **Injury x loaded side:** $P = 0.002$ Injury x location: NS Location x loaded side: NS	975.08 ± 27.39	987.29 ± 19.40	992.61 ± 25.14	951.92 ± 29.05

Data represent the marginal mean ± standard deviation of each measure. 95% confidence intervals are calculated for each main effect. The CIs are calculated in reference to uninjured, contralateral-to-loaded, and lateral levels of the injury, loaded side, and location factors, respectively.

Table 2

Osteoarthritis and Cartilage

Epiphysis and subchondral bone plate microarchitecture

edge) influenced the indentation modulus (E_i). Since a covariate describing location within the subchondral bone plate was not significant ($P = 0.057$), we used mixed model ANOVA without the covariate to test whether injury and loaded side effect E_i. Neither injury ($P = 0.052$ [−0.02, 3.64 GPa]), loaded side ($P = 0.338$ [−1.45, 1.94 GPa]), nor their interaction affected Ei (Fig. 4(D), Table III).

Distinct metabolic changes are evident in synovial fluid from injured limbs

We compared synovial fluid metabolic profiles from injured, sham-injured, and contralateral-to-injured limbs. 3,402 metabolites were detected across all synovial fluid samples. Five

Measure	Control		Injured	
	Contralateral-to-sham	**Sham-Loaded**	**Contralateral-to-injured**	**Loaded to injury**
Proximal tibia epiphysis				
Indentation Modulus (GPa) Injury: $P = 0.052$ 95%CI: (−0.02, 3.64) *Loaded side*: NS 95%CI: (−1.45, 1.94) Injury x loaded side: NS	18.33 ± 1.36	16.90 ± 3.05	19.47 ± 1.41	19.39 ± 2.76
Calcein to Bone Surface (%) ***Mouse***: $P = 0.013$ Limb (Mouse): NS Injury: NS 95%CI: (−16.32, 13.03) ***Loaded side***: $P = 0.005$ 95%CI: (−13.07, −2.84) Location: NS 95%CI: (−1.8, 6.10) Injury x loaded side: NS Injury x location: NS Location x loaded side: NS	46.10 ± 16.35	34.54 ± 17.01	40.85 ± 13.00	36.50 ± 9.08
Alizarin to Bone Surface (%) Mouse: NS ***Limb(Mouse)***: $P = 0.001$ Injury: NS 95%CI: (−9.68, 17.88) Loaded side: NS 95%CI: (−13.86, 13.69) Location: NS 95%CI: (1.19, 8.93) Injury x loaded side: NS Injury x location: NS Location x loaded side: NS	42.28 ± 18.84	33.44 ± 19.82	37.63 ± 12.66	46.30 ± 23.26
Distal femur				
Osteoclast number per bone marrow area (1/mm^2) ***Injury***: $P = 0.017$ 95%CI: (0.287, 2.420) Loaded side: NS 95%CI: (−0.669, 1.028) Injury x loaded side: NS	−9.22 ± 1.39	−9.13 ± 1.43	−7.96 ± 1.33	−7.69 ± 0.58
Osteoclast number per bone surface (1/mm) ***Injury***: $P = 0.016$ 95%CI: (0.284, 2.319) Loaded side: NS 95%CI: (−0.607, 0.919) Injury x loaded side: NS	−5.82 ± 1.28	−5.89 ± 1.27	−4.75 ± 1.30	−4.37 ± 0.58

Data represent the marginal mean ± standard deviation of each measure. Osteoclast number densities are natural log-transformed. Mouse numbers per group vary per measure: indentation modulus (injured n = 8, control n = 8); calcein-to-bone-surface and alizarin-to-bone-surface (injured n = 7, control n = 8); osteoclast measurements (injured n = 8, control n = 7). 95% confidence intervals are calculated for each main effect. The CIs are calculated in reference to uninjured, contralateral-to-loaded, and lateral levels of the injury, loaded side, and location factors, respectively.

Table 3

Osteoarthritis and Cartilage

Subchondral bone modulus, bone formation, and osteoclast number density

metabolites were considered undetected and removed (zero median intensities).

Comparison of injured, sham-injured and contralateral-to-injured reveals dysregulated metabolites

One-way ANOVA detected significantly dysregulated metabolites. PCA, PLS-DA and hierarchical clustering detected only minimal group differences. However, due to the subjectivity of hierarchical clustering[37] and the need to understand which metabolic pathways are shared between limbs (i.e., injured & sham-injured, injured & contralateral-to-injured, injured & contralateral-to-injured & sham-injured), further analysis was needed. Therefore, we employed *ensemble clustering*[38] to remove the subjectivity from metabolite clustering. Before cluster analyses, the median intensity of each metabolite in each group was determined. Clustering validation on 3,397 metabolites found that 9 clusters were optimum. Ensemble clustering (Supplementary Data Figure S12) combined with the mummichog algorithm found primary bile acid biosynthesis, purine metabolism, porphyrin metabolism, arachidonic acid metabolism, steroid hormone biosynthesis, fatty acid elongation and degradation, glycosphingolipid biosynthesis, glycosaminoglycan degradation, alanine, aspartate and glutamate

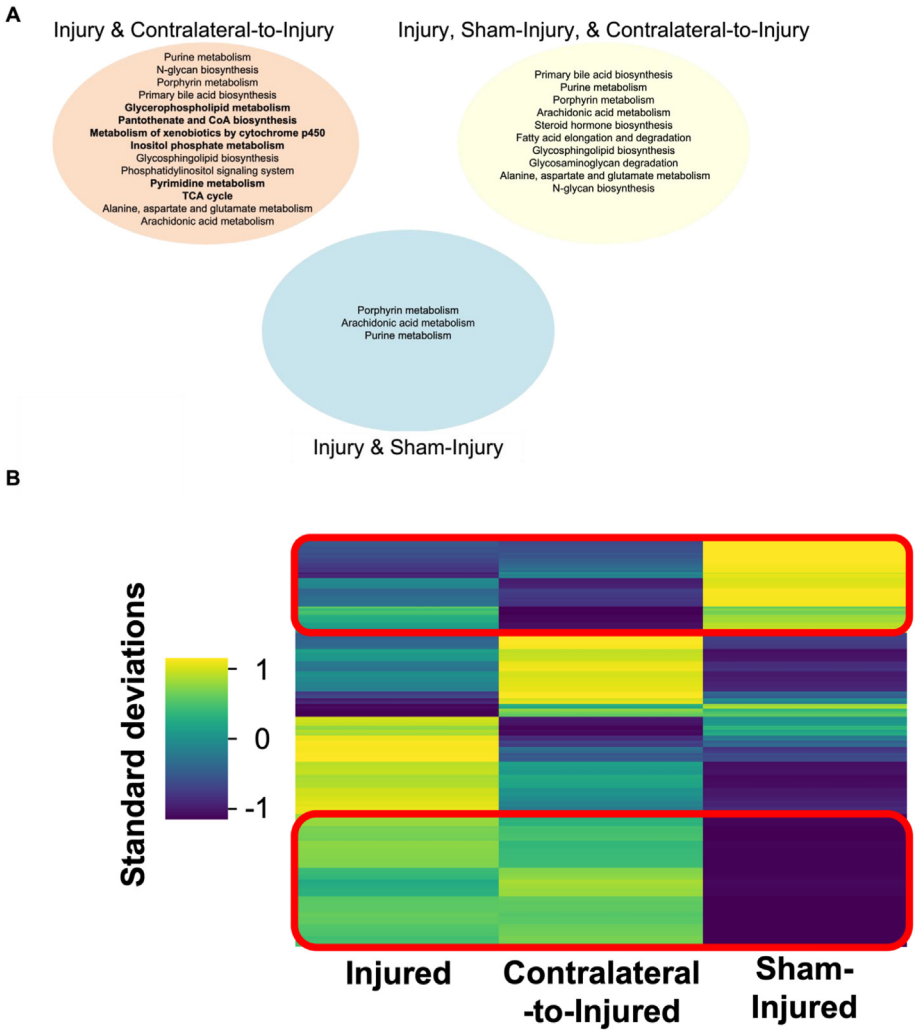


Fig. 5

Osteoarthritis and Cartilage

Ensemble clustering pathway analysis results and heatmap showing the identification of potential dysregulated metabolites A) Venn diagram of key synovial fluid metabolic pathways between injured, sham-injured, and contralateral-to-injured limbs. Bolded pathways indicated pathways specific to a systemic response. B) Heatmap analysis of metabolite clusters identified by ensemble clustering of injured, contralateral-to-injured, and sham-injured synovial fluid. Two example regions highlighted showing how distinct differences in metabolites can be identified using heatmap analysis.

metabolism, and N-glycan biosynthesis [Fig. 5(A)]. Heatmap analyses showed distinct differences in median intensities between the sham-injured and both injured and contralateral-to-injured groups [Fig. 5(B)].

Injured and sham-injured synovial fluid have distinct metabolic profiles

Because significant features were detected from ensemble clustering analyses and heatmap analysis confirmed differences in median metabolite intensities between injured, sham-injured, and contralateral-to-injured groups, we compared specific metabolites within these groups. Univariate analysis of injured vs sham-injured synovial fluid revealed 148 significant metabolites. Injured limbs had 98 upregulated and 50 downregulated metabolites compared with sham-injured limbs, after correction for false discovery rate[23]. Porphyrin metabolism was upregulated while steroid hormone biosynthesis and purine metabolism were down-regulated. PCA revealed distinct grouping of injured and sham-injured metabolic profiles apart from one outlier and was associated with 57.9% of the variability. The outlier was an injured limb which clustered with sham-injured limbs in PCA. PLS-DA revealed distinct groupings of injured and sham-injured metabolic profiles and was associated with 31.9% of the variability. Similarly, hierarchical clustering revealed clear grouping of injured vs sham-injured limbs, except for the same outlier detected by PCA.

Clustering validation indicated that 3 clusters was appropriate [Fig. 3(D)]. The top ten ensemble clustering outputs (Supplementary Data Figure S26) combined with the mummichog algorithm found porphyrin metabolism, arachidonic acid metabolism, and purine metabolism [Fig. 5(A)].

Injured and contralateral-to-injured limbs have minor differences in synovial fluid metabolic profiles

Univariate analysis of injured vs contralateral-to-injured groups found no significant metabolic features. PCA also indicated similar metabolic profiles for the first five components. However, PLS-DA revealed distinct clustering of injured and contralateral-to-injured limbs, with all but one metabolic profile grouping appropriately. Hierarchical clustering revealed no distinct groupings.

Two clusters were deemed optimal from clustering validation. Ensemble clustering found that injured and contralateral-to-injured limbs show altered purine metabolism, N-glycan biosynthesis, porphyrin metabolism, primary bile acid biosynthesis, glycerophospholipid metabolism, pantothenate and CoA biosynthesis, metabolism of xenobiotics by cytochrome p450, Inositol phosphate metabolism, glycosphingolipid biosynthesis, phosphatidylinositol signaling system, pyrimidine metabolism, TCA cycle, alanine, aspartate and glutamate metabolism, and arachidonic acid metabolism (Supplementary Data Figure S40).

Discussion

Early therapeutic interventions are needed to prevent or slow the progression of PTOA. In this study, we address several critical gaps in the early response (i.e., 7 days) of the injured joint, including (1) the response of subchondral bone tissue modulus to joint injury and (2) which bone structural, material, and metabolic outcomes are local (i.e., injured joint only) or systemic (i.e., injured and contralateral-to-injured).

Epiphyseal and subchondral bone microarchitecture both undergo bone loss 7 days after joint injury. Previous studies with this murine injury model also show reduced epiphyseal bone microarchitecture 7–10 days after injury[6–10]. However, our study found a 10.8% decrease in BV/TV and a 5.5% decrease in Tb.Th compared to 18–40%, and 18–24% decreases in these measures, respectively, from other studies[6,8–10]. Previous work reports 3–7% decrease in SCB.Th 7 days after joint injury[8,39], but we detected a larger (~12%) decrease. A potential explanation for these differences is that we studied skeletally mature mice (19-weeks old), whereas the previous studies utilized skeletally immature mice (10–11 weeks old)[6,8–10]. These results demonstrate that early changes to the epiphysis and subchondral bone plate after injury are likely sensitive to skeletal maturity.

Bone undergoes transient thinning after joint injury which then reverses[6–10]. The sclerotic bone of later-stage OA is less stiff[6–10]. However, the initial changes to subchondral bone tissue material properties after joint injury have not been reported[40,41]. We found that injury did not significantly impact subchondral bone modulus ($P = 0.052$). However, our study may be underpowered to detect these changes. The possibility that subchondral bone modulus increases soon after joint injury is important for considering the impacts of the injury on joint loading and cellular mechanotransduction[42,43].

Changes to bone structure and material properties can result from altered bone deposition, resorption, or both. Therefore, we assessed osteoclast number density and quantified the epiphyseal mineralizing surface. Our results showed an increase in osteoclast number density but not bone formation surface following joint injury. These results demonstrate that the early bone loss in our mouse model is primarily attributable to increased bone resorption.

Our experimental design allowed us to ask whether early bone changes following traumatic injuries affected the contralateral limb. We found that bone microarchitecture decreased and osteoclast number increased for both injured and contralateral-to-injured limbs. Injury and loaded side had additive effects of similar scale on early bone loss for epiphyseal BV/TV, BMD, and Tb.Th. These results improve our understanding of mouse models of PTOA because there are clear impacts to the biological and mechanical environments of both knees soon after the joint injury. Future studies should utilize sham-injured mice as controls for each time point to avoid confounding effects from systemic responses to injury. Importantly, it is not understood if changes to the contralateral-to-injured limb are transient or if they later progress towards PTOA as in the injured limb. It is also not known whether other rodent models of PTOA (e.g., DMM, ACLT) produce similar contralateral limb effects at early timepoints, since the surgical incision confounds the early response.

Synovial fluid is integral to joint health, serving as a lubricant for joint articulation and a nutrient source for joint tissues[44,45]. This study contributes to a growing body of work that demonstrates that distinct shifts occur in synovial fluid metabolism in the first week post joint injury[25] and are consistent with shifts in whole joint metabolism[46]. Our synovial fluid metabolic univariate analysis revealed that 148 metabolites were dysregulated between injured and sham-injured knees. Ensemble analysis, an analytic tool introduced to synovial fluid metabolomics in this report, found that injured and contralateral-to-injured limbs shared many common pathways. These findings do not contradict the univariate analysis, because while ensemble clustering identifies metabolites that are common between groups, it does not identify the direction (i.e., upregulated or downregulated) of any differences between the groups.

We also wanted to understand which pathways were common to injured and contralateral-to-injured limbs, since these data would inform which metabolic shifts are systemic. Several pathways were common to injured and contralateral-to-injured limbs but not injured, contralateral-to-injured, and sham-injured limbs, indicating that there were systemic shifts in metabolism after injury. Taken together, univariate and ensemble data suggest that there are pathways specific to the injured limb at 7d after injury, but also that many metabolic shifts extend to the other joint. These data suggest that the metabolic response to joint injury is very rapid and by 7 days after injury is systemic. To elucidate metabolic shifts specific to injury, future studies are needed that evaluate time points even earlier than 7 days.

Our study had several limitations. The non-invasive mouse injury model does not allow differentiation between the effects of injurious-level loading and ACL rupture on subchondral bone changes. However, there was not a significant correlation between peak load and any bone measures. We were unable to directly confirm ACL rupture for the injured limbs because of the synovial fluid extraction procedure which can inadvertently transect the ACL. However, we verified ACL rupture by the characteristic release in compressive load [Fig. 1(F)][7,8] and laxity changes compared to the contralateral joint. Previous studies show that the release in compressive load indicates ACL rupture, as verified by later dissection[7,8]. Another limitation is that embedding bone in PMMA significantly stiffens bone tissue compared with the hydrated condition[32]. However, preparing the subchondral bone plate for microscale modulus measurement required stabilizing this small structure with an infiltrating embedding material. This study was focused on the early response to joint injury. Additional timepoints would provide useful information about the trajectory of changes to subchondral bone and synovial fluid metabolism. Another important limitation was the small sample size ($n = 8$/group; $N = 16$). Changes in subchondral bone modulus may have required additional mice for detection.

In summary, this study finds that acute bone loss 7 days after joint injury occurs in the injured and contralateral-to-injured limbs, and that these changes are accompanied by dysregulated synovial fluid metabolism. Our results implicate rapidly changing structural and biological environments within both injured and

contralateral-to-injured joints that has the potential for influencing the progression to PTOA.

Author contributions

Experimental design: BDH, RKJ, CMH; Data collection: BDH, CD; Data analysis and interpretation: BDH, CD, CMH; Manuscript drafting: BDH, CMH; Revision of manuscript: all authors; Approval of manuscript: all authors.

Conflict of interest

The authors have no conflicts to disclose.

Role of funding sources

The work was supported by the National Institutes of Health (NIAMS R01AR073964 (RKJ), NIGMS P20GM103474 (CMH)) and the National Science Foundation (CMMI-2120239 (CMH), 1554708 (RKJ)). This work represents the views of the authors and not necessarily those of the sponsors.

Acknowledgments

This research was made possible by the Department of Mechanical & Industrial Engineering and the College of Engineering at the Montana State University. We appreciate assistance with microCT analyses from the Center for Advanced Orthopedic Studies μCT Core at Beth Israel Deaconess Medical Center as well as assistance with histological sample preparation from Maria Jerome.

Supplementary data

Supplementary data to this article can be found online at https://doi.org/10.1016/j.joca.2022.09.002.

References

1. Thomas AC, Hubbard-Turner T, Wikstrom EA, Palmieri-Smith RM. Epidemiology of posttraumatic osteoarthritis. J Athl Train 2017;52(6):491–6, https://doi.org/10.4085/1062-6050-51.5.08.
2. Cinque ME, Dornan GJ, Chahla J, Moatshe G, LaPrade RF. High rates of osteoarthritis develop after anterior cruciate ligament surgery: an analysis of 4108 patients. Am J Sports Med 2018;46(8):2011–9, https://doi.org/10.1177/0363546517730072.
3. Kramer WC, Hendricks KJ, Wang J. Pathogenetic Mechanisms of Posttraumatic Osteoarthritis: Opportunities for Early Intervention 2011, www.ijcem.com.
4. Anderson DD, Chubinskaya S, Guilak F, Martin J, Oegema T, Olson S, *et al*. Post-traumatic osteoarthritis: improved understanding and opportunities for early intervention. J Orthop Res 2011;29(6):802–9, https://doi.org/10.1002/jor.21359.
5. Hsia AW, Jbeily EH, Mendez ME, Cunningham H, Biris K, Bang H, *et al*. Post-traumatic osteoarthritis progression is diminished by early mechanical unloading and anti-inflammatory treatment in mice. Osteoarthritis Cartilage 2021;29(12):1709–19, https://doi.org/10.1016/j.joca.2021.09.014.
6. Anderson MJ, Diko S, Baehr LM, Bodine SC, Christiansen BA. Contribution of mechanical unloading to trabecular bone loss following non-invasive knee injury in mice. J Orthop Res 2016, https://doi.org/10.1002/jor.23178. Published online January 30.
7. Lockwood KA, Chu BT, Anderson MJ, Haudenschild DR, Christiansen BA. Comparison of loading rate-dependent injury modes in a murine model of post-traumatic osteoarthritis. J Orthop Res 2014;32(1):79–88, https://doi.org/10.1002/jor.22480.
8. Christiansen BA, Anderson MJ, Lee CA, Williams JC, Yik JHN, Haudenschild DR. Musculoskeletal changes following non-invasive knee injury using a novel mouse model of post-traumatic osteoarthritis. Osteoarthritis Cartilage 2012;20(7):773–82, https://doi.org/10.1016/j.joca.2012.04.014.
9. Khorasani MS, Diko S, Hsia AW, Genetos D, Haudenschild D, Christiansen B. Effect of alendronate on post-traumatic osteoarthritis induced by anterior cruciate ligament rupture in mice. Arthritis Res Ther 2015;17(1), https://doi.org/10.1186/s13075-015-0546-0.
10. Wegner AM, Campos NR, Robbins MA, Haddad A, Cunningham H, Yik J, *et al*. Acute changes in NADPH oxidase 4 in early post-traumatic osteoarthritis. J Orthop Res 2019;37(11):2429–36, https://doi.org/10.1002/jor.24417.
11. Stock JT. Wolff's law (bone functional adaptation). In: The International Encyclopedia of Biological Anthropology. John Wiley & Sons; 2018:1–2, https://doi.org/10.1002/9781118584538.ieba0521.
12. Maycas M, Esbrit P, Gortázar AR. Molecular mechanisms in bone mechanotransduction. Histol Histopathol 2017;32(8):751–60, https://doi.org/10.14670/HH-11-858.
13. Mazur CM, Woo JJ, Yee CS, Fields A, Acevedo C, Bailey K, *et al*. Osteocyte dysfunction promotes osteoarthritis through MMP13-dependent suppression of subchondral bone homeostasis. Bone Research 2019;7(1), https://doi.org/10.1038/s41413-019-0070-y.
14. Alliston T, Hernandez CJ, Findlay DM, Felson DT, Kennedy OD. Bone marrow lesions in osteoarthritis: what lies beneath. J Orthop Res 2018;36(7):1818–25, https://doi.org/10.1002/jor.23844.
15. Mcmahon M, Block JA. In: The Risk of Contralateral Total Knee Arthroplasty after Knee Replacement for Osteoarthritis 2003;vol. 30, www.jrheum.org.
16. Christiansen BA, Emami AJ, Fyhrie DP, Satkunananthan PB, Hardisty MR. Trabecular bone loss at a distant skeletal site following noninvasive knee injury in mice. J Biomech Eng 2015;137(1), https://doi.org/10.1115/1.4028824.
17. White MS, Brancati RJ, Lepley LK. Relationship between altered knee kinematics and subchondral bone remodeling in a clinically translational model of ACL injury. J Orthop Res 2022;40(1):74–86, https://doi.org/10.1002/jor.24943.
18. Yik JH, Hu Z, Christiansen BA, Haudenschild DR. Early transient induction of IL-6 in a mouse joint injury model. Osteoarthritis Cartilage 2013;21:S235–6, https://doi.org/10.1016/j.joca.2013.02.484.
19. Swärd P, Frobell R, Englund M, Roos H, Struglics A. Cartilage and bone markers and inflammatory cytokines are increased in synovial fluid in the acute phase of knee injury (hemarthrosis) - a cross-sectional analysis. Osteoarthritis Cartilage 2012;20(11):1302–8, https://doi.org/10.1016/j.joca.2012.07.021.
20. Marcucci G, Iantomasi T, Brandi ML, Vincenzini MT. Oxidative Stress in Bone Remodeling: Role of Antioxidants.
21. Vashishth D, Gibson GJ, Khoury JI, Schaffler MB, Kimura J, Fyhrie DP. Influence of Nonenzymatic Glycation on Biomechanical Properties of Cortical Bone 2001.
22. das Neves Borges P, Vincent TL, Marenzana M. Automated assessment of bone changes in cross-sectional micro-CT studies of murine experimental osteoarthritis. PLoS One 2017;12(3), https://doi.org/10.1371/journal.pone.0174294.

23. McCulloch K, Huesa C, Dunning L, Litherland G, Van T Hof R, Lockhart J, *et al*. Accelerated post traumatic osteoarthritis in a dual injury murine model. Osteoarthritis Cartilage 2019;27(12): 1800–10, https://doi.org/10.1016/j.joca.2019.05.027.
24. Patti GJ, Yanes O, Siuzdak G. Innovation: metabolomics: the apogee of the omics trilogy. Nat Rev Mol Cell Biol 2012;13(4): 263–9, https://doi.org/10.1038/nrm3314.
25. Hahn AK, Wallace CW, Welhaven HD, Brooks E, McAlpine M, Christiansen BA, *et al*. The microbiome mediates epiphyseal bone loss and metabolomic changes after acute joint trauma in mice. Osteoarthritis Cartilage 2021;29(6):882–93, https://doi.org/10.1016/j.joca.2021.01.012.
26. Wallace CW, Hislop B, Hahn AK, Erdogan AE, Brahmachary PP, June RK. Correlations between Metabolites in the Synovial Fluid and Serum: A Mouse Injury Study. doi:10.1101/2021.08.30.458234
27. Olah T, Madry H. The osteochondral unit: the importance of the underlying subchondral bone. In: Cartilage Restoration 2018:13–22.
28. Souza RL de, Matsuura M, Eckstein F, Rawlinson SCF, Lanyon LE, Pitsillides AA. Non-invasive axial loading of mouse tibiae increases cortical bone formation and modifies trabecular organization: a new model to study cortical and cancellous compartments in a single loaded element. Bone 2005;37(6): 810–8, https://doi.org/10.1016/j.bone.2005.07.022.
29. Bouxsein ML, Boyd SK, Christiansen BA, Guldberg RE, Jepsen KJ, Müller R. Guidelines for assessment of bone microstructure in rodents using micro-computed tomography. J Bone Miner Res 2010;25(7):1468–86, https://doi.org/10.1002/jbmr.141.
30. Schindelin J, Arganda-Carreras I, Frise E, Kaynig V, Longair M, Pietzsch T, *et al*. Fiji: an open-source platform for biological-image analysis. Nat Methods 2012;9:676–82.
31. Vahidi G, Flook H, Sherk V, Mergy M, Lefcort F, Heveran CM. Bone biomechanical properties and tissue-scale bone quality in a genetic mouse model of familial dysautonomia. Osteoporos Int 2021;32(11):2335–46, https://doi.org/10.1007/s00198-021-06006-1/Published.
32. Bushby AJ, Ferguson VL, Boyde A. Nanoindentation of bone: comparison of specimens tested in liquid and embedded in polymethylmethacrylate. J Mater Res 2004;19(1):249–59, https://doi.org/10.1557/jmr.2004.19.1.249.
33. Kim S, Hwang J, Xuan J, Jung YH, Cha HS, Kim KH. Global metabolite profiling of synovial fluid for the specific diagnosis of rheumatoid arthritis from other inflammatory arthritis. PLoS One 2014;9(6), e97501, https://doi.org/10.1371/journal.pone.0097501.
34. Carlson AK, Rawle RA, Adams E, Greenwood MC, Bothner B, June RK. Application of global metabolomic profiling of synovial fluid for osteoarthritis biomarkers. Biochem Biophys Res Commun 2018;499(2):182–8, https://doi.org/10.1016/j.bbrc.2018.03.117.
35. Domingo-Almenara X, Montenegro-Burke JR, Ivanisevic J, Thomas A, Sidie J, Teav T, *et al*. XCMS-MRM and METLIN-MRM: a cloud library and public resource for targeted analysis of small molecules. Nat Methods 2018;15(9):681–4, https://doi.org/10.1038/s41592-018-0110-3.
36. Li S, Park Y, Duraisingham S, Strobel F, Khan N, Soltow Q, *et al*. Predicting network activity from high throughput metabolomics. PLoS Comput Biol 2013;9(7), https://doi.org/10.1371/journal.pcbi.1003123.
37. Aggarwal CC, Procopiuc C, Wolf JL, Yu PS. Fast Algorithms for Projected Clustering 1999.
38. Ronan T, Qi Z, Naegle KM. Avoiding common pitfalls when clustering biological data. Sci Signal 2016;9(432):1–13, https://doi.org/10.1126/scisignal.aad1932.
39. Maerz T, Newton MD, Fleischer M, Hartner S, Gawronski K, Junginger L, *et al*. Traumatic joint injury induces acute catabolic bone turnover concurrent with articular cartilage damage in a rat model of posttraumatic osteoarthritis. J Orthop Res 2021;39(9):1965–76, https://doi.org/10.1002/jor.24903.
40. Ji M, Yu Q. Primary osteoporosis in postmenopausal women. Chronic Diseases and Translational Medicine 2015;1(1):9–13, https://doi.org/10.1016/j.cdtm.2015.02.006.
41. Manitta L, Fayolle C, Olive L, Berteau JP. Nanoindentation of subchondral bone during osteoarthritis pathological process using atomic force microscopy. In: International Symposium on Computer Methods in Biomechanics and Biomedical Engineering 2019:505–17.
42. Klein-Nulend J, van der Plas A, Semeins CM, Ajubi N, Erangos J, Nijweide P, *et al*. Sensitivity of osteocytes to biomechanical stress in vitro. Faseb J 1995;9(5):441–5, https://doi.org/10.1096/fasebj.9.5.7896017.
43. Fritton SP, Weinbaum S. Fluid and solute transport in bone: flow-induced mechanotransduction. Annu Rev Fluid Mech 2009;41(1):347–74, https://doi.org/10.1146/annurev.fluid.010908.165136.
44. Blewis ME, Nugent-Derfus GE, Schmidt TA, Schumacher BL. A model of synovial fluid lubricant composition in normal and injured joints. Eur Cell Mater 2007;13(1):26–39.
45. Jay GD, Torres JR, Warman ML, Laderer MC, Breuer KS. The Role of Lubricin in the Mechanical Behavior of Synovial Fluid 2007, www.pnas.orgcgidoi10.1073pnas.0608558104.
46. Haudenschild DR, Carlson AK, Zignego DL, Yik JHN, Hilmer JK, June RK. Inhibition of early response genes prevents changes in global joint metabolomic profiles in mouse post-traumatic osteoarthritis. Osteoarthritis Cartilage 2019;27(3):504–12, https://doi.org/10.1016/j.joca.2018.11.006.